Received July 22, 2019, accepted August 13, 2019, date of publication August 28, 2019, date of current version September 12, 2019.

Digital Object Identifier 10.1109/ACCESS.2019.2936259

Online Fatigue Estimation and Prediction of Switching Device in Urban Railway Traction Converter Based on Current Recognition and Gray Model

LEI WANG[1], (Member, IEEE), WEIHUA XU[2], SHENYI LIU[1], RUICHANG QIU[3], AND CHUNMEI XU[1]

[1]School of Electrical Engineering, Beijing Jiaotong University, Beijing 100044, China
[2]Global Energy Interconnection Research Institute Company Ltd., Beijing 102209, China
[3]Beijing Engineering Research Center of Electric Rail Transportation, Beijing Jiaotong University, Beijing 100044, China

Corresponding author: Lei Wang (leiwang@bjtu.edu.cn)

This work was supported by the Fundamental Research Funds for the Central Universities under Grant E18JB00080.

ABSTRACT It is difficult to estimate and predict the fatigue state of switchgear in traction converter of urban Electric Multiple Unit (EMU). At the same time, this is just the purpose of this paper. Firstly, the power loss and junction temperature of the device are analyzed by using the results of electro-thermal simulation and actual working conditions. Then, a novel Bi-directional accelerated fatigue test (BAFT) is proposed, and the data obtained from BAFT are used to establish a fitting fatigue model for a specific switch device. BAFT data enable the fatigue interaction between Insulated Gate Bipolar Transistor (IGBT) and Free Wheeling Diode (FWD) to be displayed in the common switching device module, and the interaction is represented by an acceleration factor. In the fatigue model, the service life and fatigue state of the equipment is related to the equivalent fatigue current which is used to generate the fatigue. The equivalent fatigue current is observed by the proposed analysis identification model. The historical data of fatigue values are subjected to Gray Model (GM) (2, 1) for trend prediction, and then the service time of the switch device is calculated using the predicted fatigue values from GM (2, 1). The examples presented in this paper are based on recorded field data.

INDEX TERMS Switching device, traction converter, fatigue estimation, lifetime prediction.

ABBREVIATIONS AND NOMENCLATURE

GM	Gray model
TC	Traction Converter
EMU	Electric Multiple Unit
IGBT	Insulated Gate Bipolar Transistor
FWD	Free Wheeling Diode
CTE	Coefficient of Thermal Expansion
AFT	Accelerated Fatigue Test
SAFT	Single-directional Accelerated Fatigue Test
BAFT	Bi-directional Accelerated Fatigue Test
EMI	Electromagnetic Interference

The associate editor coordinating the review of this manuscript and approving it for publication was Jiajie Fan.

i_U, i_V, i_W	Current outputs of TC
U_{dc}	DC voltage input of TC
T_j	Junction temperature
T_{jQ}	Junction temperature of IGBT
T_{jD}	Junction temperature of FWD
ΔT_{jQ}	Junction temperature variation of IGBT
ΔT_{jD}	Junction temperature variation of FWD
R_{th}	Thermal resistance
$R_{thj\text{-}c\_IGBT}$	Thermal resistance between the IGBT die and device case
$R_{thj\text{-}c\_FWD}$	Thermal resistance between the FWD die and device case
T_{amb}	Ambient temperature
I_{eq}	Equivalent current amplitude through the device or fatigue current
N_f	The service life of the device

p, q	Coefficients to show the accelerating effect from FWD actions on the device
α	Acceleration factor
i_{G}	IGBT current
i_{D}	FWD current
I_{test1}, I_{test2}	The currents used in BAFT
U_{CESat0}	Initial saturation voltage drop of the device
U_{CESat}	Saturation voltage drop of the device
F	Cumulative failure rate
$F_1(x)$, $F_2(x)$, $F_{1500}(x)$, $F_{1200}(x)$, $F_{900}(x)$	The functional relationship between F and the number of cycle times x under various conditions
λ_1, k_1, λ_2, k_2	Parameters in Weibull distribution
i_{d} and i_{q}	The TC current output after transformation
I_{M}	The amplitude of i_{U}, i_{V}, i_{W}
θ_{e}	Field orientation angle,
$i_{\mathrm{Du\_t}}$, $i_{\mathrm{Dl\_t}}$, $i_{\mathrm{Dl\_b}}$, $i_{\mathrm{Du\_b}}$, $i_{\mathrm{Gu\_t}}$, $i_{\mathrm{Gl\_t}}$, $i_{\mathrm{Gl\_b}}$, $i_{\mathrm{Gu\_b}}$	FWD and IGBT currents in a different stage
S_{u}, S_{l}	Switching functions
$\hat{\Psi}_{\mathrm{r}}$	Rotor field flux
L_{m}, L_{r}, R_{r}, P	Motor parameters
ω_{sl}^{*}	Reference of slip frequency
T_{e}, T_{e}^{*}	Electromagnetic torque
i_{qs}, i_{ds}	Motor stator currents after transformation
M, M (t)	Damage degree M of a switching device
D_{i}	The damage increment of i_{th} operating day
$H^{(0)}(\mathrm{k})$, $H^{(1)}(\mathrm{k})$	The sequences in GM (2, 1)
d_1, d_2, ∇	The operators in GM(2,1)
T_{s}	Sampling time interval
β_1, β_2, β_3	Coefficients in the difference equation of GM (2, 1)

I. INTRODUCTION

The urban rail transit system is an important and friendly way of tourism in the metropolis. Considering that it will not cause traffic congestion, air pollution, and increase passenger traffic, etc. Electric multi-unit (EMU) is one of the important subsystems of urban rail transit. Transportation system and traction converter (TC) in EMU provide power and electric braking force with the help of traction motor. In TC, its switching device is more likely to fail than other components [1], [2]. According to field statistics, the faults or failure of switching devices accounted for 10% to 20% of the total number of faults, which is even higher for the EMUs with a total distance of more than 105 kilometers. In many cases, the failure of switching devices is caused by fatigue [2]. If fatigue state can be predicted, the failure rate of switching device can be greatly reduced by manual maintenance or replacement [4] [5].

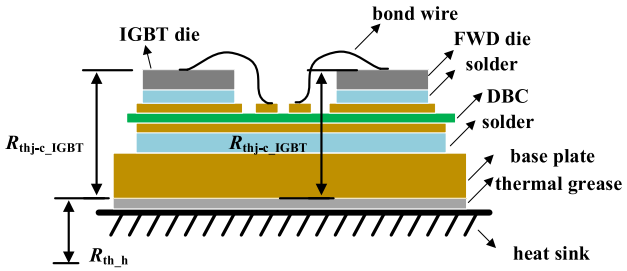

FIGURE 1. The internal structure of a switching device.

Switching devices in TC usually appear in packaging modules, which are composed of IGBT and FWD. Fatigue of switch devices mainly occurs in package failure, including bonding wire liftoffs and solder layer crack [6], [7]. Bonding wire liftoffs and solder layer cracking are caused by shear thermal stress, which is generated by temperature change inside the device. Switching device works periodically. When the device (actually the IGBT in the device) is turned on, the current flows through it; when the device is turned off, the current is cut off. When the current flows through the device, the flowing current will generate heat because of the impedance (resistance, etc.) inside the device. In other cases, no heat is produced at all. This means that the equipment will be heated when it turns on and cooled when it is turned off. IGBTs and FWD are on and off with high switching frequency (kHz) in operation. There are conduction losses, turn-on losses, and turn-off losses. Conduction, Turn-on and turn-off losses can cause loss of the PN junction, so the test in this paper measures the loss of the PN junction. Physically, the switching device consists of multiple layers (as shown in Fig. 1), and the coefficient of thermal expansion (CTE) of each layer is different. The intermittent heating and cooling process mean that the internal temperature of the device (not only IGBT junction temperature T_{j}, but the temperature of every single layer) increases and decreases accordingly. This temperature change is caused by internal thermal resistance (e.g. $\mathrm{R_{thj\text{-}c\_IGBT}}$ and $\mathrm{R_{thj\text{-}c\_FWD}}$ in Fig. 1) and heat flow. Because of the difference of CTE, the change of temperature will cause shear thermal stress, and shear thermal stress will lead to lift-offs and cracks [5]. Lift-offs and cracks are the two main forms of fatigue. Internal liftoffs and cracks cannot be observed externally due to packaging; however, several sensitive parameters can be used as fatigue characteristics to indirectly show the development of peeling and cracking. In other cases, peeling and cracking can be estimated under certain thermal cycles and temperature changes (obtained from mission profiles). Therefore, the model can be built based on Fatigue Feature observation or temperature offset counting.

For the fatigue-related modes, various electrical and thermal parameters can be selected as fatigue characteristics, such as the duration of IGBT saturation voltage drop (U_{CESat}) [8], SOA [6], thermal resistance (R_{th}) IGBT junction and device substrate [9], IGBT gate threshold voltage [10]. These methods are based on the one-to-one relationship between fatigue eigenvalues and fatigue levels.

As for temperature-related methods, various methods have been introduced to obtain junction temperature T_j [11], [12] [13], and then the value or trend of T_j is counted by a specially designed algorithm. A well-known algorithm is the rain-flow counting method [14]. This method is based on the fact that the switching device has a limited and fixed load-carrying capacity of T_j cycle under certain operating conditions. Each cycle causes fatigue to accumulate inside the device. When the cumulative fatigue reaches above the fatigue threshold, the switch device will fail. The fatigue threshold and working conditions are also one-to-one correspondence.

However, for various reasons, the above fatigue models are seldom applied to actual EMU situations.

A. IT IS HARD TO DETECT THOSE FATIGUE SIGNATURES AND T_j WITH SUFFICIENT ACCURACY, AND ADDITIONAL CIRCUITS ARE NECESSARY

Switching devices in TC always withstand continuous high voltage and load current. In this case, serious EMI exists. EMI makes it difficult to detect sensitive parameters and T_j with sufficient accuracy. However, the switching frequency of switch devices in TC varies with the speed of EMU, so it is not easy to design appropriate filters to eliminate EMI.

More importantly, special circuits are needed to detect fatigue characteristics and T_j. It is better to embed these circuits into trigger units of the switching device. However, considering that the current manufacturers of trigger units do not provide such additional circuits in their products, it is not easy to achieve detection.

B. ONLY IGBT IS CONSIDERED IN THE FATIGUE MODEL, WHICH IS NOT ENOUGH

Obviously, it is impossible to detect the one-to-one relationship mentioned above in the field operation, because such a process must last as long as the expected service life - more than 30 years. But it is usually not certain whether the IGBT can continue to be used for 30 years, so we need to fit the model to predict how much life the IGBT has. Therefore, the accelerated fatigue test (AFT) is needed. AFT uses predefined cumulative damage stress testing equipment (DUT) and obtain data showing the fatigue characteristics of DUT.

In the switching device, the current can flow through it in two directions, as shown in Fig. 2. C and E are the external terminals of the device. In Fig. 2 (a), the current flows from the internal IGBT through C to E; in Fig. 2 (b), the current flows from E to C through the internal FWD. In the AFT process, the DUT is heated by the test current flowing through it. However, traditional AFT only considers the test current in one direction, that is, the direction shown in

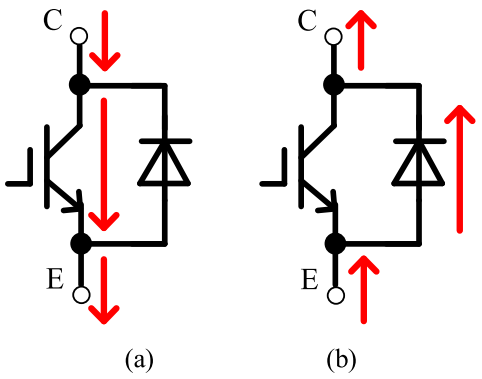

FIGURE 2. The current direction difference between IGBT and FWD.

Fig. 2 (a) [16]–[18]. This is mainly because IGBT is more vulnerable in devices, so cumulative damage of IGBT means cumulative damage of DUT. Indeed, IGBT actions should be considered in AFT, but FWD actions can also lead to cumulative damage to DUT (based on the analysis in Part II). The traditional one-way AFT (SAFT) should be improved to bi-directional AFT (BAFT), in which the test current flows through IGBT and FWD. Data obtained from BAFT accurately show cumulative damage effects caused by IGBT and FWD.

C. ONLY A FIXED OPERATING CONDITION IS CONSIDERED IN THE FATIGUE MODEL, WHICH IS ALSO NOT ENOUGH

The fatigue model proposed by existing methods needs stable and fixed operating conditions because it is based on the results of AFT with fixed experimental conditions [15]–[18]. Therefore, the existing model is not fully applicable when the actual field operation conditions have been changing, which is exactly the case of the TC application. For example, in actual TC operation, due to the movement of EMU, the switching device undergoes changing ambient temperature, while the ambient temperature remains constant in AFT [17]; moreover, the switching frequency (i.e., the number of turns on and off in one second) and the current of the switching device continuously change with the change of EMU speed or passenger capacity, while the traditional AFT only considers constant switching frequency and constant test current [18] [19].

This paper tries to put forward an on-line estimation method and prediction scheme for Fatigue Grade of switching devices, which is suitable for the application of a traction converter of EMU. Initially, a novel bi-directional AFT (BAFT) test program is proposed. Using the data obtained from BAFT, the acceleration factor is introduced into the fatigue model to illustrate the effect of FWD action on the cumulative damage process of the device. In BAFT, DUT is also affected by various bidirectional test currents to ensure that the fatigue model is more applicable under different working conditions (or varying current output). More importantly, environmental temperature is also taken into account in the fatigue model.

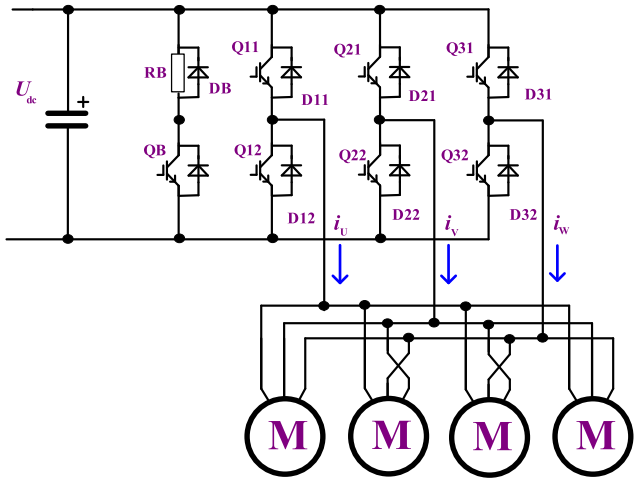

(a)

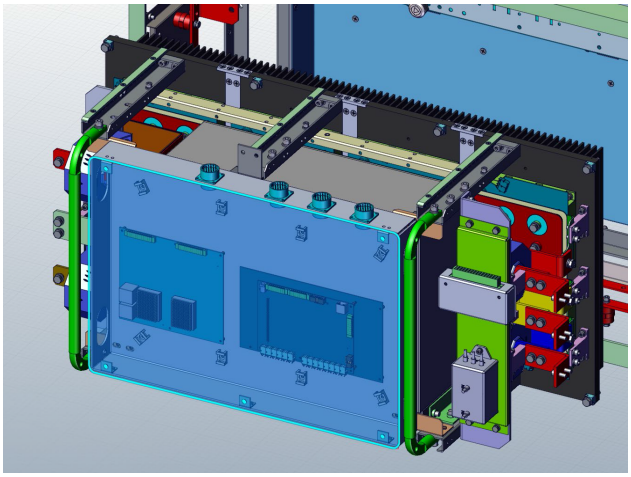

(b)

FIGURE 3. The electrical (a) topology and (b) layout of TC's power module.

In order to realize on-line estimation of fatigue level, we propose an analytical model to observe FWD and IGBT currents, which are used to construct damage increments. Finally, the damage increment sequence is input into the second-order GM (2, 1) to predict the fatigue degree in the future. All the data used in the example comes from the actual field application.

II. THE EFFECT OF FWD AND IGBT ACTIONS ON DEVICE ACCUMULATED DAMAGE DURING TC OPERATION

Fig. 3 (a) shows the power circuit topology of TC. There are six switch devices, which are placed in a compact power module, as shown in Fig. 3 (b). Q_{11}-Q_{32} is IGBT, D_{11}-D_{32} is FWD, U_{dc} is DC voltage input, i_U, i_V, i_W is three-phase AC current output from TC to four traction motors M behind it. QB, RB, and DB constitute a brake energy consumption branch. Q_{11}-Q_{32} and D_{11}-D_{32} are usually packaged in six device modules, which are installed on the radiator. QB and DB are not often used, so only cumulative damage and fatigue of Q_{11}-Q_{32} and D_{11}-D_{32} are considered.

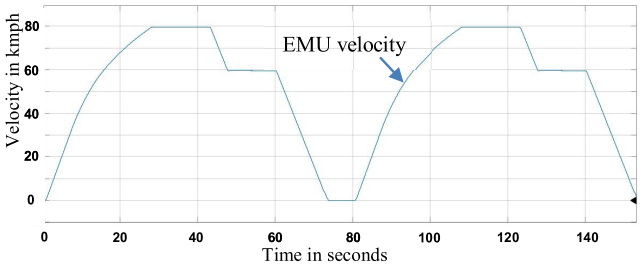

FIGURE 4. The vehicle velocity curve used in the simulation.

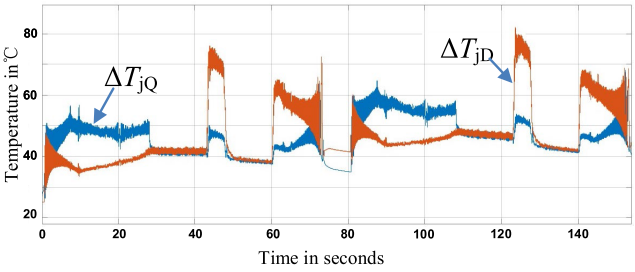

FIGURE 5. The simulated junction temperatures of Q32 and D32 under AW0.

The internal temperature of the switching device is calculated by electro-thermal simulation under given operating conditions. In the simulation, the EMU undergoes two operation cycles, as shown in Fig. 4. In Fig. 4, EMUs are in traction stage at 0s-24s and 80s-104s, and in traction stage at 43s-48s, 60s-77.5s, 123s-128s, and 140s-157.5s. The traction stage means that the EMU speed increases due to the traction torque produced by the traction motor, and the electric braking stage means that the EMU speed decreases due to the braking torque produced by the traction motor. When the traction motor does not produce torque, the EMU speed remains basically unchanged. When the EMU moves through inertia, the operation stage is called the sliding stage.

The simulation results of switching devices in TC applications are shown in Fig. 5. The switching devices we use are 1500A/3300V, the switching frequency is 57 Hz-1000Hz (according to vehicle speed control and using SVPWM modulation scheme [20]) TC capacity is 1050KA, U_{dc} is 1500V, the maximum deceleration of EMU is -1.2m/s^2, the maximum average acceleration is 0.4m/s^2, the weight of a single vehicle in EMU is 36 tons, the capacity of traction motor is 210 kW, the maximum traction force is 1630Nm, and the maximum system. Power 1500 Nm. Four motors are installed in each vehicle, and there are six vehicles in each EMU. The ambient temperature is set to 25 °C. In the simulation, the R_{th} of the radiator is calculated by SOLIDWORKS, and the R_{th} of the switching device is obtained by the transient thermal resistance curve, which is given in the device data table.

In Fig.5, the maximum change of FWD junction temperature (ΔT_{jD}) is 56.3°C, and that of IGBT junction temperature (ΔT_{jQ}) is 39.7°C. The change of junction temperature will seriously affect the service life of devices [21] [22]. According to the data obtained from LESIT [21] and CIPS08 [22]

TABLE 1. The ΔT_j of Q_{32} and D_{32} under different load conditions.

Load condition	ΔT_{jQ}	ΔT_{jD}
AW0	39.7°C	56.3°C
AW2	52.6°C	72.1°C
AW3	60.9°C	87.2°C

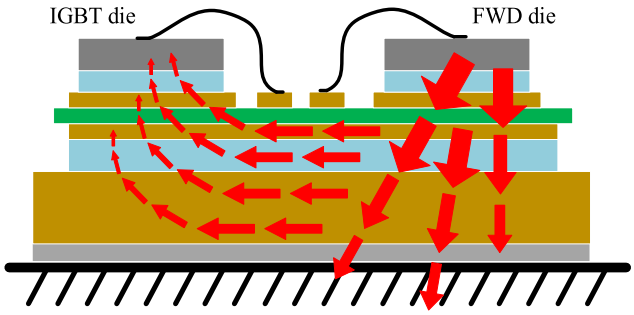

FIGURE 6. The heat flow with FWD actions.

experiments, the change of junction temperature and average junction temperature (T_m) are the key factors that affecting the cumulative damage process. Table 1 shows the maximum values of ΔT_{jQ} and ΔT_{jD} under different load conditions. ΔT_{jQ} and ΔT_{jD} are affected by various factors, such as power loss of IGBT and FWD, heat dissipation conditions, thermal resistance between junction and radiator, etc. Basically, T_m is mainly determined by ambient temperature (T_{amb}), ΔT_{jQ} and ΔT_{jD}. In Table 1, ΔT_{jQ} and ΔT_{jD} increase with vehicle load, which means that there is an approximate one-to-one relationship between ΔT_{jQ} and load conditions, and between ΔT_{jD} and load conditions. Finally, T_m is determined by T_{amb} and load conditions.

In Fig. 5, it should be noted that ΔT_{jQ} is higher in traction stage than ΔT_{jD} but lower in braking stage. In the braking stage of high-speed area (43s-48s, 123s-128s), ΔT_{jD} will increase much faster than ΔT_{jQ}. This is due to the fact that according to the requirements of EMU motion, more power is needed in the high-speed braking stage than in the traction stage, and the braking power mainly flows through FWD rather than IGBT [23].

It should be noted that the heat generated by the FWD die during FWD operation also passes through all layers of the switch device, and the heat is also transferred to the IGBT core (as shown in Fig. 6). This means that ΔT_{jD} affects the temperature change of each layer in the device and ΔT_{jQ}. As mentioned above, thermal stress is caused by temperature change and the difference in CTE, so ΔT_{jD} also results in thermal stress in the solder layer, DBC and even IGBT core. This is why FWD action should never be neglected in the fatigue process of switchgear, especially in the case of TC.

Through FWD action, IGBT aging faster and fatigue process faster than only IGBT action. If the cumulative damage state of DUT is still represented by the cumulative damage state of IGBT (as is the case in the existing reference [3]–[5]), the acceleration effect of FWD action must be considered.

III. THE AFT AND FATIGUE MODEL OF SWITCHING DEVICE CONSIDERING FWD ACTIONS

The fatigue model shows the relationship between fatigue accumulation and fatigue degree. The fatigue of the switching device is directly affected by the load condition of the vehicle. TC current output reflects the load level and this current flow through the switch device completely. Therefore, there is a one-to-one relationship between TC current output and fatigue level of switching devices, as well as the relationship between current and fatigue level of devices and service life of devices. More importantly, environmental temperature T_{amb} should also be considered. One of the basic problems in power cycle testing is the difficulty in choosing test conditions. Target T_j is a function of dissipated energy. For a given chip technology, dissipated energy is determined by the forward current and T duration in the test and the thermal resistance of the test device. Therefore, it is very difficult to repeat the test under exactly the same test conditions, but it is more difficult to select test parameters for different T_j values under the same current and heating time. If these parameters have an effect on the test results, these parameters must be taken into account in the life model [24]. Therefore, the changes in average temperature, amplitude, range, and frequency are not considered in the test.

$$N_f = f(I_{eq}) \times g(T_{amb}) \tag{1}$$

In eq. (1), N_f is the cycle number that a device could withstand before its failure, we denote N_f as the service life of the device; I_{eq} is the equivalent current amplitude through the device, f and g are both certain functions.

A. THE ACCUMULATED DAMAGE-ACCELERATING EFFECT FROM FWD ACTIONS AND BAFT

The accelerating effect from FWD actions means that device service life is shortened, as shown in eq. (2).

$$N_{f2} = pN_{f1} \tag{2}$$

In eq. (2), N_{f2} is the actual service life with FWD actions, and N_{f1} is the lifetime when only IGBT actions are considered. p is a coefficient which shows the accelerating effect. For better applicability, we express eq. (1) in the current form, as shown in eq. (3).

$$I_{eq}^2 = i_G^2 + \alpha^2 i_D^2 \tag{3}$$

In (3), i_G is the current of IGBT, i_D is that of FWD, and α is acceleration factor. The fatigue of semiconductor device is caused by the accumulation of thermal stress effect, the relationship between thermal stress effect and current is squared, therefore the currents here are in RMS (Root-Mean-Square) form and the square operation exists. α is actually used to indicate the influence of i_D, and the form of α has no decisive influence, so it is expressed in the form of square.

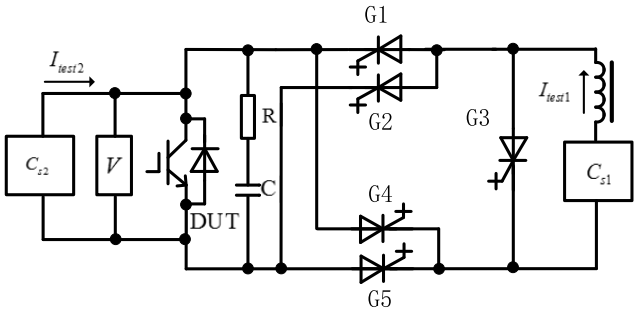

FIGURE 7. The test platform layout of BAFT.

In order to obtain α, we propose a new type of AFT with bidirectional fatigue current (BAFT), and the BAFT test platform is shown in Fig. 7. In Fig. 7, G1-G5 is the auxiliary GTO; I_{test1} is the fatigue current (i.e. the current that produces fatigue in DUT and I_{test2} is used for T_{jQ} and T_{jD} observation). R and C form an absorption branch to protect DUT by eliminating voltage spikes. When G1 and G5 are turned on, I_{test1} flows through the IGBT part inside the DUT. When G2 and G4 open, I_{test1} flows through the FWD part of the DUT. When G1, G2, G4, and G5 are all closed, additional G3 is used to provide I_{test1}'s continuation route. C_{S1} and C_{S2} produce I_{test1} and I_{test2} respectively. During BAFT, the ambient temperature (about 25°C in our experiment) was recorded and I_{test2} was 1.5A, which was basically less than 0.1% of the rated current of DUT according to experience. The cycle time was 12 seconds and the duty cycle was 48%. In BAFT, the cycle number of IGBT and FWD is equal, so only half of the total action number is considered. It should be noted that the heating effect of I_{test2} has been tested, and I_{test2} will hardly cause any observed additional junction temperature rise in DUT because of its very short duration (100ms). DUT is placed in a real TC power module during BAFT and then connected to the test platform.

The cumulative fatigue rate curve obtained from BAFT is shown in Fig. 8 and from SAFT. In Fig. 8, I_{test1} is 1500A, and the cumulative failure rate is calculated by the observed U_{CESat} [13], as shown in eq. (4). Since the PN junction voltage drop is inversely proportional to the temperature [24], the temperature is obtained by the current supplied by C_{S2}, that is, U_{CESat} can be measured. The test was interrupted when the PN junction of the switch reached 125 °C. The on-time of the IGBT and diode is determined by whether the junction temperature reaches this temperature.

$$F = \frac{U_{\text{CESat}} - U_{\text{CESat0}}}{U_{\text{CESat0}}} \tag{4}$$

In eq. (4), F is the cumulative failure rate, U_{CESat0} is the initial on-state saturation voltage drop of the new DUT, and U_{CESat} is the present on-state voltage drop. When U_{CESat} reaches 1.2 U_{CESat0}, F is defined as 1. It should be noted here that U_{CESat} increases by 5% or 20%, depending on the measurement accuracy of U_{CESat} [24]. The device in this paper can be used normally with an increase of 5% and failures will occur only with an increase of 20%. The mathematical

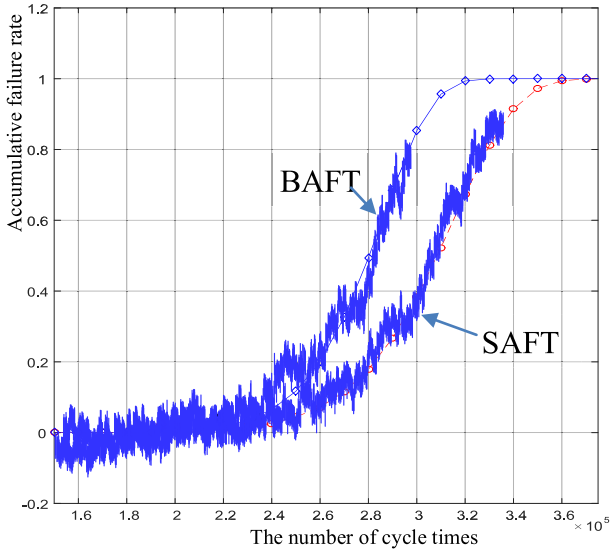

FIGURE 8. The curves obtained from BAFT and SAFT under 1500A.

analytic relationship between F and cycle number x can be fitted as follows:

$$F_1(x) = 1 - e^{-\left(\frac{x}{283769}\right)^{15.05}} \tag{5}$$

For comparison, conventional single-directional AFT (SAFT) [16]–[18] is also carried out. Since the fatigue process of switching device follows the Weibull distribution law [6], [9], [10], [25], the resulting curve is fitted to be:

$$F_2(x) = 1 - e^{-\left(\frac{x}{317254}\right)^{1298}} \tag{6}$$

To derive α, we define an intermediate variable q, which is obtained from the quotient between the medians of $F_1(x)$ and $F_2(x)$, as shown in eq. (7).

$$q = \frac{\lambda_2 \Gamma(1 + \frac{1}{k_2})}{\lambda_1 \Gamma(1 + \frac{1}{k_1})} \tag{7}$$

In eq. (7), Γ is gamma function, λ_1, λ_2 and k_1, k_2 are parameters in F_1(x) and F_2(x), while λ_1 =283769, k_1 =15.05, and λ_2 =317254, k_2 =12.98. With these values, q is calculated to be 1.1125.

From the difference between BAFT and SAFT, it gives

$$\begin{cases} I_{\text{eq}} = q i_{\text{G}} \\ i_{\text{G}} = i_{\text{D}} \end{cases} \tag{8}$$

Considering that $i_{\text{G}} = i_{\text{D}}$ =1500A and q =1.1125, $\alpha = \sqrt{0.2377} = 0.4875$. From eq. (3), it means that FWD actions accelerate 23.77% of the accumulated damage speed.

B. ANALYTICAL FATIGUE MODEL

Other BAFTs are carried out with different I_{test1}. The curves are shown in Fig. 9. Under the I_{test1} of 1200A and 900A, the mathematical analytical models of F vs. x are:

$$F_{1200}(x) = 1 - e^{-\left(\frac{x}{508785}\right)^{801}} \tag{9}$$

$$F_{900}(x) = 1 - e^{-\left(\frac{x}{918264}\right)^{596}} \tag{10}$$

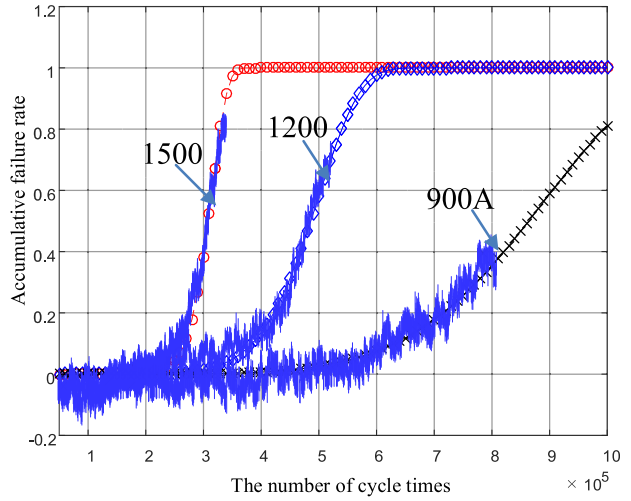

FIGURE 9. The curves obtained from BAFT under different fatigue currents.

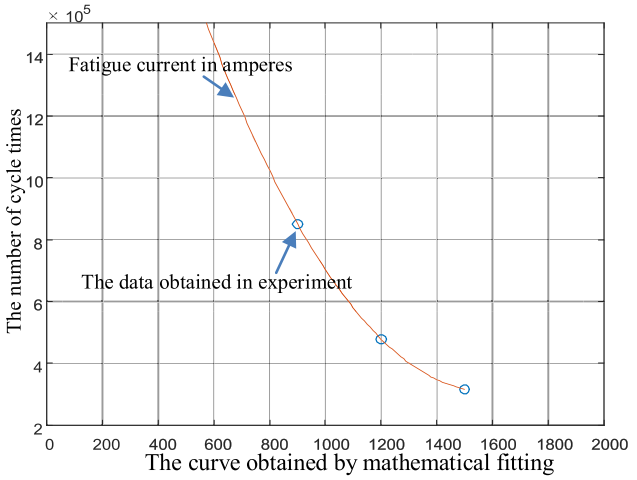

FIGURE 10. The experimental result of BAFT and the fitted curve.

And it is also known from eq. (6) that

$$F_{1500}(x) = 1 - e^{-\left(\frac{x}{317254}\right)^{1288}} \tag{11}$$

In eq. (9) - eq. (11), the F_{1500}(x), F_{1200}(x), and F_{900}(x) is cumulative failure rate under the I_{test1} of 1500A, 1200A, and 900A, respectively, with the medians of them to be 304890, 479170 and 851580. The medians are denoted to be the corresponding device service life N_{f}.

Finally after fitting calculation, eq. (1) is expressed as:

$$N_{\text{f}} = \left(1.17\, I_{\text{test1}}^2 - 3697.11\, I_{\text{test1}} + 3.23^{*}10^6\right) \times e^{k\left(\frac{1}{T_{\text{mmb}}} - \frac{1}{25}\right)} \tag{12}$$

In eq. (12), k is an Arrhenius coefficient. According to Arrhenius's rule (the temperature increase of 10°C implies that the service life is shortened by half), k is calculated to be 60.65. The experimental and fitted curve is shown in Fig.10.

Considering the RMS calculation scheme, hence

$$I_{\text{test1}} = \sqrt{2} I_{\text{eq}} \tag{13}$$

It gives

$$N_{\text{f}} = (2.34 I_{\text{eq}}^2 - 5228.35 I_{\text{eq}} + 3.23^{*}10^6) \times e^{60.65\left(\frac{1}{T_{\text{amb}}} - \frac{1}{25}\right)} \tag{14}$$

IV. THE ONLINE RECOGNITION MODEL OF FATIGUE CURRENT OF THE SWITCHING DEVICE

Although i_{G} is equal to i_{D} in BAFT experiment, they are not equal in actual TC operation during traction and braking stages. In order to obtain the actual N_{f} of the equipment, it is necessary to calculate the actual I_{eq} according to eq. (3), in which the values of i_{G} and i_{D} are indispensable. Unfortunately, only the AC current output of TC (i.e. i_{U}, i_{V}, i_{W}) is detectable, not i_{G} and i_{D}, because current detectors can only be installed at the output of TC, so it is impossible to detect device current due to hardware implementation difficulties.

Therefore, i_{G} and i_{D} need to be calculated from i_{U}, i_{V}, and i_{W}. Here, we propose the analysis and recognition models of i_{G} and i_{D}.

Because i_{U}, i_{V}, and i_{W} are AC values, they should be transformed to DC values through Clarke and Park transforms [26], as shown in eq. (15), where i_{d} and i_{q} are DC currents obtained after DC transforms.

$$\begin{pmatrix} i_{\text{d}} & i_{\text{q}} \end{pmatrix}' = C \begin{pmatrix} i_{\text{U}} & i_{\text{V}} & i_{\text{W}} \end{pmatrix}' \tag{15}$$

In eq. (15), the transformation matrix C is

$$C = \frac{2}{3} \begin{pmatrix} \cos(\theta_{\text{e}}) & \cos(\theta_{\text{e}} - \frac{2}{3}\pi) & \cos(\theta_{\text{e}} + \frac{2}{3}\pi) \\ \sin(\theta_{\text{e}}) & \sin(\theta_{\text{e}} - \frac{2}{3}\pi) & \sin(\theta_{\text{e}} + \frac{2}{3}\pi) \end{pmatrix} \tag{16}$$

θ_{e} is the field orientation angle, which is generated by the vector control scheme of TC [26]. I_{M} is the amplitude value of i_{U}, i_{V}, and i_{W} and therefore it gives

$$I_{\text{M}} = \sqrt{i_{\text{d}}^2 + i_{\text{q}}^2} \tag{17}$$

In the coasting stage of EMU, TC outputs no current, so the current recognition model is only required to obtain i_{G} and i_{D} in the traction stage and the electrical braking stage.

A. IGBT AND FWD CURRENT RECOGNITION SCHEME IN TRACTION STAGE

In the traction stage, TC acts as an inverter, and the current recognition model could be expressed in eq. (18) - eq. (21).

$$i_{\text{Gu\_t}} = \begin{cases} S_{\text{u}} I_{\text{M}} \sin(\theta_{\text{e}}), & \theta_{\text{e}} \in [0, \pi) \\ 0, & \theta_{\text{e}} \in [\pi, 2\pi) \end{cases} \tag{18}$$

$$i_{\text{Du\_t}} = \begin{cases} S_{\text{l}} I_{\text{M}} \sin(\theta_{\text{e}}), & \theta_{\text{e}} \in [\pi, 2\pi) \\ 0, & \theta_{\text{e}} \in [0, \pi) \end{cases} \tag{19}$$

$$i_{\text{Gl\_t}} = \begin{cases} S_{\text{u}} I_{\text{M}} \sin(\theta_{\text{e}}), & \theta_{\text{e}} \in [\pi, 2\pi) \\ 0, & \theta_{\text{e}} \in [0, \pi) \end{cases} \tag{20}$$

$$i_{\text{Dl\_t}} = \begin{cases} S_{\text{l}} I_{\text{M}} \sin(\theta_{\text{e}}), & \theta_{\text{e}} \in [0, \pi) \\ 0, & \theta_{\text{e}} \in [\pi, 2\pi) \end{cases} \tag{21}$$

In eq. (18) - eq. (21), i means instantaneous value of current, the subscript _t means traction stage, the subscript

G/D means IGBT/FWD current, and the subscript u/l means the upper or lower device(in Fig. 3, Q_{11}, Q_{21}, Q_{31} are upper IGBTs, Q_{12}, Q_{22}, Q_{32} are lower ones). S_u and S_l are the switching functions of upper and lower IGBT. When S_u/S_l is 1, it means the trigger signal of upper/lower IGBT is effective. Neglecting dead time zone, it gives

$$S_u + S_l = 1 \tag{22}$$

Considering eq. (22), eq. (19) and eq. (21) could be revised as

$$i_{Du\_t} = \begin{cases} (1 - S_u) I_M \sin(\theta_e), & \theta_e \in [\pi, 2\pi) \\ 0, & \theta_e \in [0, \pi) \end{cases} \tag{23}$$

$$i_{Dl\_t} = \begin{cases} (1 - S_u) I_M \sin(\theta_e), & \theta_e \in [0, \pi) \\ 0, & \theta_e \in [\pi, 2\pi) \end{cases} \tag{24}$$

It should be noted that the current identification model above does not distinguish three phases U, V, and W. i_{Gu_t} can be instantaneous currents of Q_{11} or Q_{21} and Q_{31}. Similarly, i_{Du_t} can belong to D_{11} or D_{21} and D_{31}. This is inaccurate because the instantaneous currents of phases U, V and W have the same magnitude, and they shift at an electric angle of 120° [26]. However, the fatigue of IGBT or FWD is not affected by the position of current angle but is seriously affected by the current amplitude. Therefore, angular displacement is not considered here.

B. IGBT AND FWD CURRENT RECOGNITION IN ELECTRICAL BRAKING STAGE

The current recognition model in electrical braking stage is given in eq. (25) to eq. (28).

$$i_{Gu\_b} = \begin{cases} (1 - S_u) I_M \sin(\theta_e), & \theta_e \in [0, \pi) \\ 0, & \theta_e \in [\pi, 2\pi) \end{cases} \tag{25}$$

$$i_{Du\_b} = \begin{cases} S_u I_M \sin(\theta_e), & \theta_e \in [\pi, 2\pi) \\ 0, & \theta_e \in [0, \pi) \end{cases} \tag{26}$$

$$i_{Gl\_b} = \begin{cases} (1 - S_u) I_M \sin(\theta_e), & \theta_e \in [\pi, 2\pi) \\ 0, & \theta_e \in [0, \pi) \end{cases} \tag{27}$$

$$i_{Dl\_b} = \begin{cases} S_u I_M \sin(\theta_e), & \theta_e \in [0, \pi) \\ 0, & \theta_e \in [\pi, 2\pi) \end{cases} \tag{28}$$

In the equations above, the subscript _b means electrical braking stage.

C. IGBT AND FWD CURRENT RECOGNITION SCHEME WITH CURRENT DETECTOR BROKEN

When anyone of the 3 current detectors is broken, i_U, i_V, i_w could no longer be all detected. The current recognition model should be revised accordingly. According to the rotor field orientation vector control scheme, it gives

$$\omega_{sl}^* = \frac{L_m R_r}{\hat{\Psi}_r L_r} i_{qs}, \tag{29}$$

where $\hat{\Psi}_r$ is the observed rotor field flux, L_m is magnetic excitation inductance, L_r is the leakage inductance of rotor, R_r is total rotor resistance, ω_{sl}^* is the reference of slip frequency, i_{qs} is the stator current along with axle q in 2-axle rotating coordination system.

Considering that

$$\hat{\Psi}_r = L_m i_{ds}, \tag{30}$$

where i_{ds} is the stator current along with axle d in 2-axle rotating coordination system, it gives

$$\omega_{sl}^* = \frac{R_r}{I_{ds} L_r} i_{qs} \tag{31}$$

The torque output T_e of a traction motor could be given as

$$T_e = \frac{3}{2}\left(\frac{P}{2}\right)\frac{L_m^2}{L_r} i_{ds} i_{qs}, \tag{32}$$

where P is the magnetic polar count of traction motor when the torque is controlled in a closed-loop system, T_e is equal to torque reference T_e^*, so it gives

$$T_e^* = \frac{3}{2}\left(\frac{P}{2}\right)\frac{L_m^2}{L_r} i_{ds} i_{qs} \tag{33}$$

By combining eq. (31) with eq. (33), it gives

$$i_{qs} = \frac{2L_r}{L_m}\sqrt{\frac{\omega_{sl}^* T_e^*}{3PR_r}} \tag{34}$$

$$i_{ds} = \frac{2\sqrt{R_r}}{\omega_{sl}^* L_m}\sqrt{\frac{\omega_{sl}^* T_e^*}{3P}} \tag{35}$$

Since that there are altogether 4 traction motors, both i_{ds} and i_{qs} is 25% of i_d and i_q. By substituting eq. (34) and eq. (35) into eq. (17), it gives

$$I_M = \frac{8}{L_m}\sqrt{\frac{R_r}{(\omega_{sl}^*)^2} + \frac{L_r^2}{R_r}}\sqrt{\frac{\omega_{sl}^* T_e^*}{3P}} \tag{36}$$

In eq. (36), it is not necessary to detect i_U, i_V, and i_w, but it requires accurate motor parameters (such as L_m, L_r, R_r, etc.). The motor parameters fluctuate with temperature, so the identification error of eq. (36) is higher than eq. (18) -eq. (28). Eq. (36) is only used when one or more current detectors are damaged.

Fig.11 to Fig.13 show the simulation results of Q_{22} currents observed during the acoustic current detector and traction phases. Fig. 11 is the i_V waveform when the current reference direction is from TC to the traction motor. When Q_{22} is triggered, i_V flows through it. The actual current waveform through Q_{22} is shown in Fig. 12, and the current observed through Q_{22} and the proposed identification model is shown in Fig. 13. It should be noted that the identified current according to eq. (20) is input to the mobile window filter to obtain a mean value to eliminate any possible current sparks. In the filter, the window width is chosen to be 0.05 Ms. Obviously, the observed current is very close to the actual value.

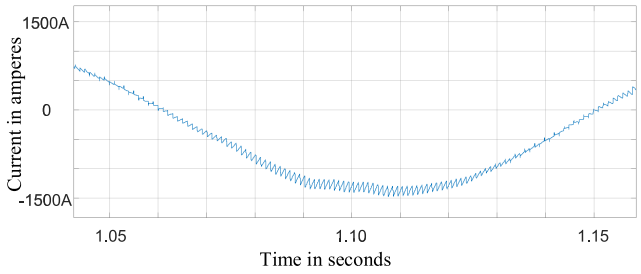

FIGURE 11. The waveform of i_V.

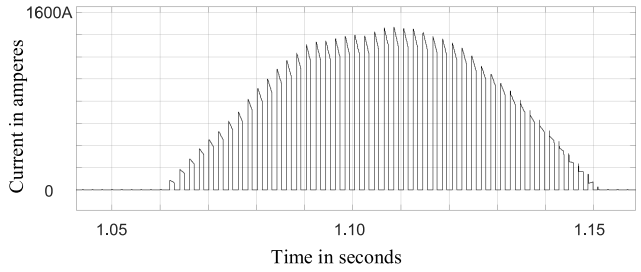

FIGURE 12. The current waveform through Q_{22}.

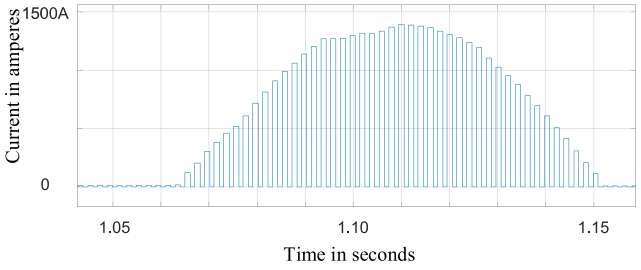

FIGURE 13. The recognized current waveform through Q_{22}.

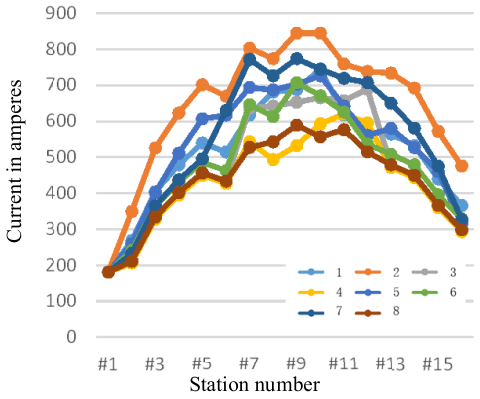

FIGURE 14. The equivalent fatigue current values that are detected in 8 rounds of upstream EMU operation.

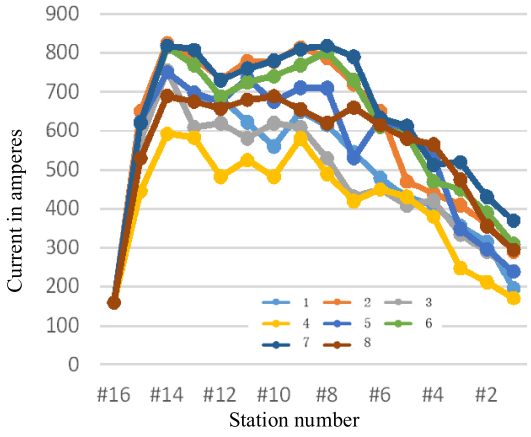

FIGURE 15. The equivalent fatigue current values that are detected in 8 rounds of downstream EMU operation.

D. THE CALCULATION OF EQUIVALENT FATIGUE CURRENT

Since that EMU takes the natural day as the basic time unit, the I_{eq} should be calculated on a daily basis. Finally, I_{eq} could be given as

$$I_{eq} = \sqrt{\sum_{j=1}^{N_a} I_{eqj}^2 \Big/ N_a} \tag{37}$$

In eq. (37), N_a is the total number of operating cycle times of the day. I_{eqj} is the equivalent fatigue current of the j_{th} operating cycle, and it should be calculated according to eq. (38). In eq. (38), N_j is the total number of action times of the device in the j_{th} operating cycle, i_{Gi} and i_{Di} is the i_{th} recognized value of IGBT and FWD current inside the device.

$$I_{eqj} = \sqrt{\sum_{i=1}^{N_t} (i_{Gi}^2 + \alpha^2 i_{Di}^2) \Big/ N_j} \tag{38}$$

V. THE ONLINE SERVICE LIFE EVALUATION APPROACH

According to eq. (14), the service life N_f can be calculated by I_{eq}, as shown in eq. (37). However, N_f is the number of actions, which is useless in practical field applications, in which the service life of the unit of days or years is required.

Based on cumulative damage theory [27], we denote the damage degree M of a switching device as

$$M = \sum_i D_i \tag{39}$$

where D_i is the damage increment of the i_{th} day, D_i is expressed by

$$D_i = \frac{N_i}{N_{fi}} \tag{40}$$

In eq. (40), N_i is the actual number of cycle times of i_{th} day, N_{fi} is the service life calculated according to eq. (14) and eq. (37).

Here comes an example. There are 16 stations along the railway line and 16 operation sections along the railway line. The total mileage is 35 kilometers. During the testing period, EMU served eight rounds. I_{eqj} values detected by eq. (18) - eq. (28) and eq. (38) are given in Fig. 14 and Fig. 15. The average ambient temperature of the day was 17.3 °C.

According to eq. (37), the final I_{eq} is calculated to be 554.8A, and N_{fi} is 3089969 according to eq. (14). N_i is 16*8=128 in a day; therefore D_i is 4.14×10^{-5}, according to eq. (40).

If M with a value of 1 means that the device is completely damaged, the EMU can run 24154 days (i.e. $(4.14\times10^{-5})^{-1}$) before the switch in TC fails. Assuming that the EMU runs eight rounds a day and 330 days a year, the EMU can run for up to 73 years.

This example only considers the fatigue state on a specific operating day. However, the fatigue process is seriously affected by the actual load conditions and ambient temperature, which are changing every day. The ''73 years'' here are calculated according to the load conditions and ambient temperature of a particular day, which is not accurate. Some advanced forecasting schemes should be applied.

VI. THE SERVICE LIFE PREDICTION SCHEME WITH 2-ORDER GRAY MODEL

Eq. (9) to eq. (11) shows that the fatigue trend of the switchgear follows the exponential characteristic. More importantly, load conditions affecting fatigue and cumulative damage processes also show similar characteristics. For example, the passenger flow in rail transit system shows a weak exponential trend similar to the Matthew effect. When there is an exponential trend, GM can better achieve the prediction [28], [29].

The value damage degree M (t) in a given time duration t is less than 1, as shown in eq. (41).

$$M(t) \in [0, \varepsilon), \quad 0 < \varepsilon < 1 \tag{41}$$

Based on eq. (41), it is very easy to construct non-negative quasi-smooth sequences with M (t) [28]. Based on this quasi-smooth sequence, GM can be constructed to predict its future value. GM belongs to different types, among which GM (1, 1) (order 1 and an independent variable) is the most popular. However, the Weibull trend in eq. (9) - eq. (11) shows a two-part exponential law with inflection points around the median point. For this special case, GM (2, 1) (order 2 and an independent variable) is more suitable. Because of the ability to construct the second-order whitening differential equation of the original data, GM (2, 1) is actually suitable for the linear combination of complex data changes and two exponential signals, which shows a two-stage exponential trend without the characteristic of general monotonous increase or decrease. This is the Weibull distribution. Considering the influence of heat flow, the fatigue accumulation in the switchgear follows the Weibull distribution. Therefore, GM (2, 1) is better when Weibull is fitted. The flow chart of grey model prediction algorithm is shown in Fig. 16.

Assuming that the input sequence of GM is $H^{(0)}$ (k) (k denotes the k_{th} sampling point); the following steps should be taken in the prediction process of GM (2, 1).

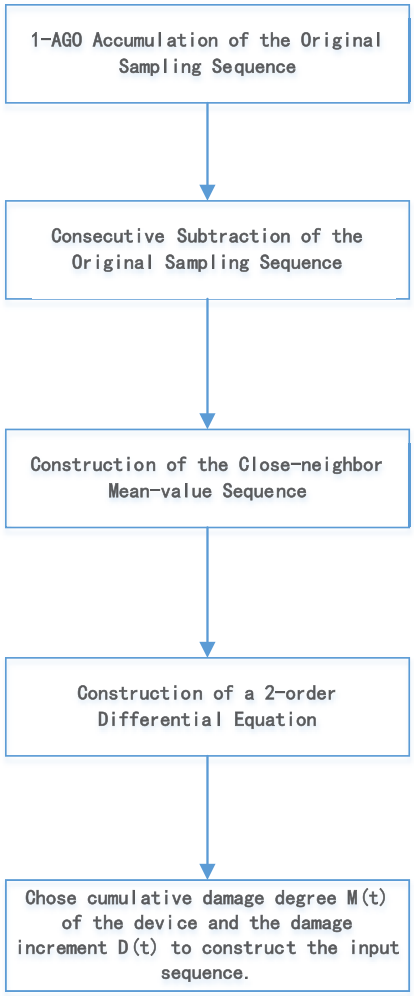

FIGURE 16. Prediction algorithm flow of grey model.

A. 1-AGO ACCUMULATION OF THE ORIGINAL SAMPLING SEQUENCE

After the 1-AGO accumulation, it gives:

$$H^{(1)} = H^{(0)}d_1 = \{H^{(1)}(1), H^{(1)}(2)...H^{(1)}(n)\}, \tag{42}$$

where d_1 is 1-AGO operator and

$$H^{(1)}(k) = \sum_{i=1}^{k} H^{(0)}(i) \tag{43}$$

In (43), $H^{(1)}$ (k) could be interpreted to be the whitened data of $H^{(0)}$ (k).

B. CONSECUTIVE SUBTRACTION OF THE ORIGINAL SAMPLING SEQUENCE

After consecutive subtraction, it gives

$$H^{(0)}d_2 = \{H^{(1)}(1)d_2, H^{(1)}(2)d_2...H^{(1)}(n)d_2\} \tag{44}$$

$$H^{(0)}(k)d_2 = H^{(0)}(k) - H^{(0)}(k-1), \tag{45}$$

where d_2 is consecutive subtraction operator.

C. CONSTRUCTION OF THE CLOSE-NEIGHBOR MEAN-VALUE SEQUENCE

The close-neighbor mean-value sequence is expressed as

$$H^{(0)} = 0.5H^{(1)}(k) + 0.5H^{(1)}(k-1) \tag{46}$$

D. CONSTRUCTION OF A 2-ORDER DIFFERENTIAL EQUATION

$$\frac{d^2}{dt^2}H^{(1)}(t) + \alpha_1\frac{d}{dt}H^{(1)}(t) + \alpha_2 H^{(1)}(t) = \alpha_3 \tag{47}$$

According to eq. (47), it gives

$$H^{(1)}(t) = L^{-1}\left[\frac{\alpha_3}{s\left(s^2+\alpha_1 s+\alpha_2\right)} + \frac{H^{(1)}(0_-)\,s + H^{(1)'}(0_-) + \alpha_1 H^{(1)}(0_-)}{s^2+\alpha_1 s+\alpha_2}\right] \tag{48}$$

Eq. (48) could not be solved by digital processors, it should be revised. With simultaneous integration of the two sides of eq. (47), it gives

$$\int_{(k-1)T_s}^{kT_s}\frac{d^2}{dt^2}H^{(1)}(t)dt + \alpha_1\int_{(k-1)T_s}^{kT_s}\frac{d}{dt}H^{(1)}(t)dt + \alpha_2\int_{(k-1)T_s}^{kT_s}H^{(1)}(t)dt = \alpha_3\int_{(k-1)T_s}^{kT_s}dt, \tag{49}$$

while T_s is the sampling interval of the processor.

Since that

$$\frac{d^2}{dt^2}H^{(1)}(t) \approx \frac{d}{dt}\left[\frac{H^{(1)}(k)-H^{(1)}(k-1)}{T_s}\right] \tag{50}$$

And

$$\frac{d}{dt}\left[\frac{H^{(1)}(k)-H^{(1)}(k-1)}{T_s}\right] = \frac{1}{T_s^2}\left[H^{(0)}(k)-H^{(0)}(k-1)\right] \tag{51}$$

It gives

$$\nabla\left(H^{(0)}(k)\right) + \beta_1 H^{(0)}(k) + \beta_2\left[0.5H^{(1)}(k)+0.5H^{(1)}(k-1)\right] = \beta_3 \tag{52}$$

In eq. (52), ∇ is a backward difference operator, and it is a difference equation. Eq. (52) could be solved by a digital processor. In it, the coefficients are

$$\beta_1 = \alpha_1 T_s,\ \beta_2 = \frac{\alpha_2}{2}T_s^2,\ \beta_3 = \alpha_3 T_s^2 \tag{53}$$

The characteristic equation of eq. (52) is

$$\left(1+\beta_1+\frac{\beta_2}{2}\right)\lambda^2 + \left(-2-\beta_1+\frac{\beta_2}{2}\right)\lambda + 1 = 0, \tag{54}$$

and the characteristic roots of eq. (52) are

$$\delta_{1,2} = \frac{2+\beta_1-\frac{\beta_2}{2} \pm \sqrt{\left(\beta_1-\frac{\beta_2}{2}\right)^2-4\beta_2}}{2\left(1+\beta_1+\frac{\beta_2}{2}\right)} \tag{55}$$

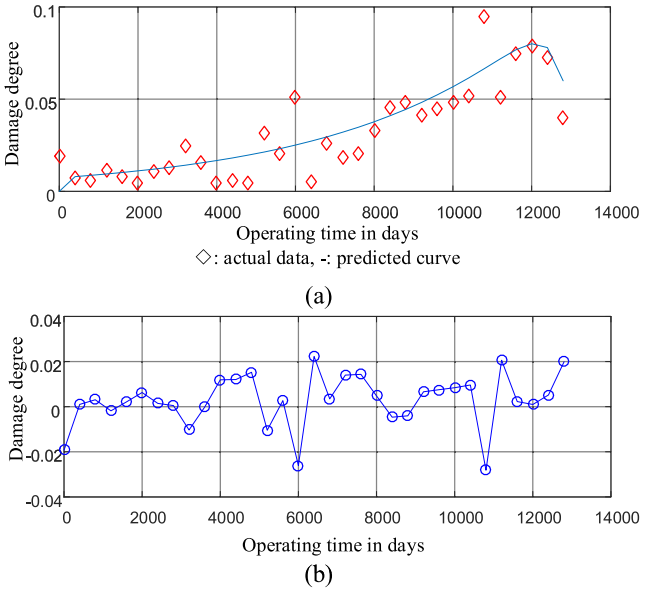

FIGURE 17. The prediction result with D to be the input.

Moreover, the coefficient vector (β_1, β_2, β_3) in eq. (52) is derived by LSM algorithm with a pseudo-inverse matrix of $(\mathrm{A}^{\mathrm{T}}\,\mathrm{A})^{-1}$:

$$\begin{pmatrix}\beta_1 & \beta_2 & \beta_3\end{pmatrix} = (A^TA)^{-1}A^TB \tag{56}$$

In eq. (56), the metrics of A and B are:

$$A = \begin{pmatrix} -H^{(0)}(2) & -0.5H^{(1)}(1)-0.5H^{(1)}(2) & 1 \\ -H^{(0)}(3) & -0.5H^{(1)}(2)-0.5H^{(1)}(3) & 1 \\ \vdots & \vdots & \vdots \\ -H^{(0)}(k) & -0.5H^{(1)}(n-1)-0.5H^{(1)}(n) & 1 \end{pmatrix} \tag{57}$$

$$B = \begin{pmatrix} \sigma(M^{(0)}(2)) \\ \sigma(M^{(0)}(3)) \\ \vdots \\ \sigma(M^{(0)}(n)) \end{pmatrix} \tag{58}$$

Since the fatigue process consists of no fluctuations or concessions, it gives

$$\left(\beta_1-\frac{\beta_2}{2}\right)^2 - 4\beta_2 > 0 \tag{59}$$

Eq. (59) is used as the constraint condition of the LSM process. With eq. (56) - eq. (58), β_1, β_2 and β_3 are derived, and eq. (52) is instantiated and then solved.

In GM (2, 1), both cumulative damage degree M (t) of the device and the damage increment D (t) could be chosen to construct the input sequence. Fig. 17 and Fig. 18 show the prediction with the input sequence of these two cases. The data in both figures are obtained from the historical record of actual field performance.

In Fig. 17, the solution to eq. (47) is

$$D(t) = 0.087e^{0.0815t} - 1.533e^{-16}e^{1.020t} - 0.075 \tag{60}$$

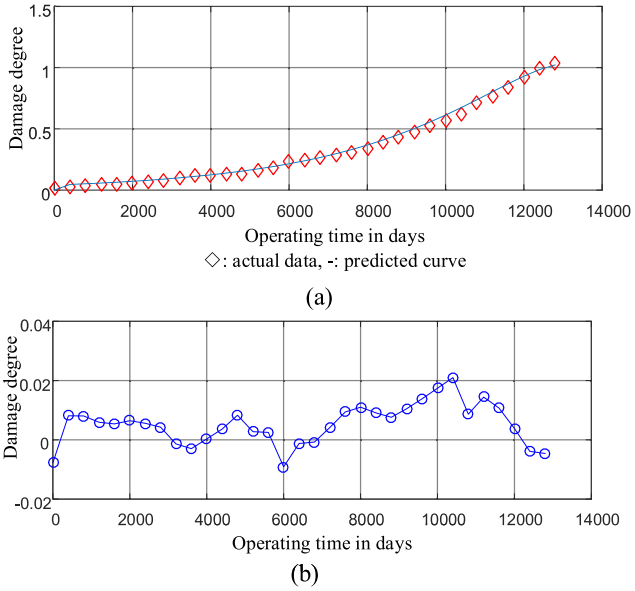

FIGURE 18. The prediction result with M to be the input.

In eq. (60), t is the operating time of traction converter in days. As for Fig. 18, the solution to eq. (47) is

$$M(t) = 0.405e^{0.148t} - 0.167e^{0.168t} - 0.253 \qquad (61)$$

Eq. (60) shows basically one-section exponential tendency because the coefficient of the second item is very small. Eq. (61) meets the 2-section distribution better. In Fig. 17, it is obvious that the error of eq. (60) is higher.

Finally, according to eq. (61), the service life is predicted to be 12474 days (when M (t) =1). This means 37.8 years. Such result is much shorter but apparently more accurate, because an EMU in urban rail transit is requiring operating 30 years, and most of them could not last much longer.

By comparing the results in Fig. 17 and Fig. 18, it is obvious that the error of the prediction results in Fig. 17 is between −0.03 and 0.02, and that in Fig. 18 is between −0.01 and 0.02. At the same time, it can be seen that the fluctuation of the result error in Fig. 18 is significantly smaller than that in Fig. 17. The number of positive and negative alternations of the result error in Fig. 17 is 7 times, while that in Fig. 18 is only 3 times. Therefore, the prediction result with M to be the input is obviously more accurate.

VII. CONCLUSION

This paper presents a new on-line fatigue assessment and prediction scheme for traction converter switchgear of urban EMU. Our goal is to predict the service life of switchgear in daily operation. A new BAFT is proposed. The data from BAFT show the fatigue characteristics more accurately. Considering the load conditions and ambient temperature, a suitable model is constructed. The proposed analytical identification model enables on-line monitoring of fatigue development. Fatigue value is helpful to calculate damage accumulation, which is the key to predict the service life of equipment by GM (2, 1).

REFERENCES

[1] S. Yang, A. Bryant, P. Mawby, D. Xiang, L. Ran, and P. Tavner, "An industry-based survey of reliability in power electronic converters," *IEEE Trans. Ind. Appl.*, vol. 47, no. 3, pp. 1441–1451, May/Jun. 2011. doi: 10.1109/TIA.2011.2124436.

[2] S. Yang, D. Xiang, A. Bryant, P. Mawby, L. Ran, and P. Tavner, "Condition monitoring for device reliability in power electronic converters: A review," *IEEE Trans. Power Electron.*, vol. 25, no. 11, pp. 2734–2752, Nov. 2010.

[3] D. Hirschmann, D. Tissen, S. Schröder, and R. W. De Doncker, "Reliability prediction for inverters in hybrid electrical vehicles," in *Proc. 37th IEEE Power Electron. Spec. Conf.*, Jeju, South Korea, Jun. 2006, pp. 1–6. doi: 10.1109/pesc.2006.1712078.

[4] H. Huang and P. A. Mawby, "A lifetime estimation technique for voltage source inverters," *IEEE Trans. Power Electron.*, vol. 28, no. 8, pp. 4113–4119, Aug. 2013. doi: 10.1109/TPEL.2012.2229472.

[5] A. T. Bryant, P. A. Mawby, P. R. Palmer, E. Santi, and J. L. Hudgins, "Exploration of power device reliability using compact device models and fast electrothermal simulation," *IEEE Trans. Ind. Appl.*, vol. 44, no. 3, pp. 894–903, May 2008. doi: 10.1109/TIA.2008.921388.

[6] G. Coquery and R. Lallemand, "Failure criteria for long term accelerated power cycling test linked to electrical turn off SOA on IGBT module. A 4000 hours test on 1200A–3300V module with AlSiC base plate," *Microelectron. Rel.*, vol. 40, nos. 8–10, pp. 1665–1670, 2000.

[7] M. Ciappa, F. Carbognani, and W. Fichtner, "Lifetime prediction and design of reliability tests for high-power devices in automotive applications," *IEEE Trans. Device Mater. Rel.*, vol. 3, no. 4, pp. 191–196, Dec. 2003. doi: 10.1109/TDMR.2003.818148.

[8] A. Oukaour, B. Tala-Ighil, B. Pouderoux, M. Tounsi, M. Bouarroudj-Berkani, S. Lefebvre, and B. Boudart, "Ageing defect detection on IGBT power modules by artificial training methods based on pattern recognition," *Microelectron. Rel.*, vol. 51, no. 2, pp. 386–391, Feb. 2011.

[9] M. Ciappa, F. Carbognani, and W. Fichtner, "Lifetime modeling of thermomechanics-related failure mechanisms in high power IGBT modules for traction applications," in *Proc. 15th IEEE Int. Symp. Power Semiconductor Devices ICs*, Apr. 2003, pp. 295–298. doi: 10.1109/ISPSD.2003.1225286.

[10] V. K. Sundaramoorthy, E. Bianda, R. Bloch, D. Angelosante, I. Nistor, G. J. Riedel, F. Zurfluh, G. Knapp, and A. Heinemann, "A study on IGBT junction temperature (Tj) online estimation using gate-emitter voltage (Vge) at turn-off," *Microelectron. Rel.*, vol. 54, no. 11, pp. 2423–2431, Nov. 2014.

[11] M. Musallam and C. M. Johnson, "Real-time compact thermal models for health management of power electronics," *IEEE Trans. Power Electron.*, vol. 25, no. 6, pp. 1416–1425, Jun. 2010. doi: 10.1109/TPEL.2010.2040634.

[12] A. Bryant, S. Yang, P. Mawby, D. Xiang, L. Ran, P. Tavner, and P. R. Palmer, "Investigation into IGBT dV/dt during turn-off and its temperature dependence," *IEEE Trans. Power Electron.*, vol. 26, no. 10, pp. 3019–3031, Oct. 2011. doi: 10.1109/TPEL.2011.2125803.

[13] Y. Avenas, L. Dupont, and Z. Khatir, "Temperature measurement of power semiconductor devices by thermo-sensitive electrical parameters—A review," *IEEE Trans. Power Electron.*, vol. 27, no. 6, pp. 3081–3092, Jun. 2012. doi: 10.1109/TPEL.2011.2178433.

[14] I. Rychlik, "A new definition of the rainflow cycle counting method," *Int. J. Fatigue*, vol. 9, no. 2, pp. 119–121, Apr. 1987.

[15] L. Fratelli, B. Cascone, G. Glannini, and G. Busatto, "Long term reliability testing of HV-IGBT modules in worst case traction operation," *Microelectron. Rel.*, vol. 39, nos. 6–7, pp. 1137–1142, Jun./Jul. 1999.

[16] M. Mermet-Guyennet, X. Perpiñá, and M. Piton, "Revisiting power cycling test for better life-time prediction in traction," *Microelectron. Rel.*, vol. 47, nos. 9–11, pp. 1690–1695, Sep./Nov. 2007.

[17] U.-M. Choi, S. Jørgensen, and F. Blaabjerg, "Advanced accelerated power cycling test for reliability investigation of power device modules," *IEEE Trans. Power Electron.*, vol. 31, no. 12, pp. 8371–8386, Dec. 2016. doi: 10.1109/TPEL.2016.2521899.

[18] V. Smet, F. Forest, J.-J. Huselstein, F. Richardeau, Z. Khatir, S. Lefebvre, and M. Berkani, "Ageing and failure modes of IGBT modules in high-temperature power cycling," *IEEE Trans. Ind. Electron.*, vol. 58, no. 10, pp. 4931–4941, Oct. 2011. doi: 10.1109/TIE.2011.2114313.

[19] A. R. de Vega, P. Ghimire, K. B. Pedersen, I. Trintis, S. Beczckowski, S. Munk-Nielsen, B. Rannestad, and P. Thøgersen, "Test setup for accelerated test of high power IGBT modules with online monitoring of VCE and VF voltage during converter operation," in *Proc. Int. Power Electron. Conf.*, May 2014, pp. 2547–2553. doi: 10.1109/IPEC.2014.6869948.
[20] Z. Shu, J. Tang, Y. Guo, and J. Lian, "An efficient SVPWM algorithm with low computational overhead for three-phase inverters," *IEEE Trans. Power Electron.*, vol. 22, no. 5, pp. 1797–1805, Sep. 2007. doi: 10.1109/TPEL.2007.904228.
[21] M. Held, P. Jacob, G. Nicoletti, P. Scacco, and M.-H. Poech, "Fast power cycling test of IGBT modules in traction application," in *Proc. 2nd Int. Conf. Power Electron. Drive Syst.*, vol. 1, May 1997, pp. 425–430. doi: 10.1109/PEDS.1997.618742.
[22] R. Bayerer, T. Herrmann, T. Licht, J. Lutz, and M. Feller, "Model for power cycling lifetime of IGBT modules—Various factors influencing lifetime," in *Proc. 5th Int. Conf. Integr. Power Electron. Syst.*, Mar. 2008, pp. 1–6.
[23] F. Du, J. H. He, L. Yu, M. X. Li, Z. Q. Bo, and A. Klimek, "Modeling and simulation of metro DC traction system with different motor driven trains," in *Proc. Asia–Pacific Power Energy Eng. Conf.*, Mar. 2010, pp. 1–4. doi: 10.1109/APPEEC.2010.5448372.
[24] J. Lutz, *Semiconductor Power Devices*. Berlin, Germany: Springer-Verlag, 2011, p. 536.
[25] R. Jiang and T. Wang, "Log-Weibull distribution as a lifetime distribution," in *Proc. QR2MSE*, Chengdu, China, 2013, pp. 813–816. doi: 10.1109/QR2MSE.2013.6625694.
[26] S. Tadakuma, I. S. Tanaka, H. Naitoh, and K. Shimane, "Improvement of robustness of vector-controlled induction motors using feedforward and feedback control," *IEEE Trans. Power Electron.*, vol. 12, no. 2, pp. 221–227, Mar. 1997. doi: 10.1109/63.558731.
[27] T. Nakagawa and M. Kijima, "Replacement policies for a cumulative damage model with minimal repair at failure," *IEEE Trans. Rel.*, vol. 38, no. 5, pp. 581–584, Dec. 1989. doi: 10.1109/24.46485.
[28] X. Zhu, S. Cui, N. Shi, and Y. Min, "Grey prediction model of motor reliability of electric vehicle," *Electr. Mach. Control*, vol. 16, no. 8, pp. 42–46, Aug. 2012.
[29] J. Yin, C. Gao, and X. Jia, "Wavelet packet analysis and gray model for feature extraction of hyperspectral data," *IEEE Geosci. Remote Sens. Lett.*, vol. 10, no. 4, pp. 682–686, Jul. 2013. doi: 10.1109/LGRS.2012.2218569.

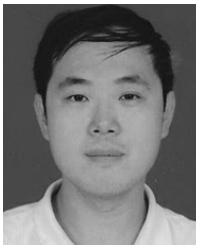

LEI WANG was born in Yantai, China, in 1982. He received the B.S. degree from the China University of Petroleum, in 2005, and the Ph.D. degree in electrical engineering from Beijing Jiaotong University, in 2010.

Since 2012, he has been a Lecturer with the Department of Electrical Engineering, Beijing Jiaotong University. His research interests include power supply configuration and power-saving technology, traction control and auxiliary power conversion, communication network and net-based monitoring, AC and DC protection, fault diagnosis and damage assessment, and project management and its applications.

WEIHUA XU received the B.Eng., M.Eng., and Ph.D. degrees in electrical engineering from North China Electric Power University, China, in 2004, 2006, and 2010, respectively.

Since 2010, she has been a Postdoctoral Fellow of the China Electric Power Research Institute, Beijing, China. In 2012, she joined the State Grid Smart Grid Research Institute, Beijing. Her research interests include UHVDC converter valve electrical design and dynamic reactive power compensation and protection of the converter in UHVDC transmission systems.

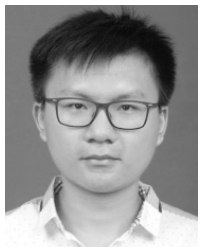

SHENYI LIU was born in Baoding, China, in 1996. He received the B.S. degree in electrical engineering from the Hebei University of Science and Technology, in 2018. He is currently pursuing the master's degree with Beijing Jiaotong University. His research interests include fault diagnosis and applications of artificial intelligence in fault diagnosis.

RUICHANG QIU was born in 1968. He received the B.S. and M.S. degrees in electrical engineering from Beijing Jiaotong University.

From 1990 to 2005, he was a Lecturer with the Department of Electrical Engineering, Beijing Jiaotong University, where he has been an Associate Professor with the Department of Electrical Engineering, since 2005. His research interests include intelligent detection technology, power electronics, and energy conversion technology and electric traction, and transmission control.

CHUNMEI XU received the Ph.D. degree from the Beijing University of Aeronautics and Astronautics, in 2004.

Since 2004, she has been a Lecturer and an Associate Professor of electrical engineering with Beijing Jiaotong University. Her research interests include rail traction drive and control, intelligent detection and control technology, rail traffic safety prediction and control, and high precision servo control systems.